Heliyon 8 (2022) e11183

Contents lists available at ScienceDirect

Heliyon

journal homepage: www.cell.com/heliyon

Research article

An *in vivo* and *in vitro* assessment of the anti-breast cancer activity of crude extract and fractions from *Prunella vulgaris* L.

Hongshan Luo [a,b], Lingjia Zhao [a,b], Yamei Li [a,b], Bohou Xia [a,b], Yan Lin [a,b], Jingchen Xie [a,b], Ping Wu [a,b], Duanfang Liao [a,b], Zhimin Zhang [a,b,*], Limei Lin [a,b,**]

[a] College of Pharmacy, Hunan University of Chinese Medicine, Changsha 410208, China
[b] Key Laboratory for Quality Evaluation of Bulk Herbs of Hunan Province, Hunan University of Chinese Medicine, Changsha 410208, China

ARTICLE INFO

Keywords:
Prunella vulgaris L.
Herb
Breast cancer
Apoptosis
Caspase

ABSTRACT

Prunella vulgaris L.(*P. vulgaris*) is a perennial herb belonging to the Labiate family and widely distributed in China, Japan, Korea and Europe. Medical monographs and previous studies have shown that *P. vulgaris* has significant anti-breast cancer activity, and its use in breast treatment has a long history. However, systematically reports about the material basis and mechanism of *P. vulgaris* on anti-breast cancer activity are limited. In the present study, we first screened the best active fraction from the crude extract (PVE) and ethanol eluted fractions of *P. vulgaris* by using MDA-MB-231, MCF-7, 4T1 cell models *in vitro* and a 4T1-BALB/c transplanted tumour mouse breast cancer model *in vivo*. Furthermore, the anti-breast cancer mechanism of the best active fraction was investigated. The results demonstrated that PVE and ethanol fractions exhibited anti-breast cancer activity, especially with the 50% ethanol eluted fraction (PV50), which effectively regulated the 4T1 cell cycle, inhibited tumour cell proliferation, and promoted cancer cell apoptosis. In case of *in vivo* assays, PV50 inhibited tumour growth and lung metastasis, as well as inducing cell apoptosis by promoting damage of nuclear DNA and increasing expression of cleaved caspase-3. In addition, the chemical compositions of PV50 were analyzed by HPLC and UPLC-MS/MS, which were identified as flavonoids, moderately polar triterpenes, and a small amount of phenolic acid. The PV50 could be applied as natural sources against breast cancer in the pharmaceutical industry. These findings provide a basis for understanding the mechanism of the anti-breast cancer activity of *P. vulgaris*.

1. Introduction

The folk Chinese tradition attributes breast cancer to the accumulation of toxins, heat, swelling and blood stasis in the body. This pathology is cited as 'breast rock' in the most ancient Chinese medical texts [1]. Triple-negative breast cancer (TNBC) is the second most common subtype of breast cancer in the world, accounting for approximately 15% of breast cancer types [2]. TNBC has a poor prognosis, high recurrence rate, high rate of metastasis, rapid progression, and low survival rate, becoming a research hotspot in recent years [3]. To date, cytotoxic chemotherapy is still the standard treatment for TNBC and other breast cancer diseases. Presently, mastectomy and chemotherapy provide the best prognosis for long-term survival, but unfortunately approximately 70% of patients are inoperable because of advanced tumor growth or bone metastasis [4]. At the same time, long-term use of drugs leads to drug resistance, losing their specific killing effect on tumour cells [5]. Therefore, new treatment strategies and methods are in urgent need of development. Natural compounds of plant origin, such as polyphenols [6] including flavonoids, tannins, curcumin, resveratrol and gallocatechin, etc.; sterol compounds of brassinosteroids [7] and their cyanoside derivatives; and vitellin, saponin, lignin, pentane and paclitaxel, all show good anticancer effects, and some have been developed into new clinical drugs (paclitaxel, docetaxel, etc.). Compared with chemotherapy and other treatments, natural products exhibit advantages of less toxicity and side effects and have gradually developed into one of the main drug classes for the treatment of cancer [8].

P. vulgaris, a medicinal and edible herb, also known as Self-heal, has a wide range of reported activities, such as clearing internal heat, improving eyesight, dispelling lumps, and reducing swelling as a traditional Chinese medicine [9]. *P. vulgaris* is rich in chemical components, among which triterpenoids, phenolic acids, flavonoids and polysaccharides are its primary active components, which exert a variety of

* Corresponding author.
** Corresponding author.
E-mail addresses: zhangzhimin8230@163.com (Z. Zhang), limei_lin@hnucm.edu.cn (L. Lin).

https://doi.org/10.1016/j.heliyon.2022.e11183
Received 29 March 2022; Received in revised form 7 June 2022; Accepted 12 October 2022
2405-8440/© 2022 Published by Elsevier Ltd. This is an open access article under the CC BY-NC-ND license (http://creativecommons.org/licenses/by-nc-nd/4.0/).

pharmacological effects such as hypolipidaemic, antitumor, anti-inflammatory, antioxidant and immune regulation effects [10, 11]. The theory of traditional Chinese medicine believes that tumours are mostly tangible masses. In addition to treatment based on the symptoms, treatment should include softening and dispelling the masses to eliminate them. The method of softening and dispelling masses is also a common treatment for tumours. In recent years, a number of clinical or preclinical studies have shown that *P. vulgaris* is effective against breast cancer, lung cancer, oesophageal cancer, gastric adenocarcinoma, etc. [12, 13].

Medical monographs and previous studies have shown that *P. vulgaris* has a long history of use in the breast and has clear anti-breast cancer activity [14]. Ruanjian Sanjie (RJSJ) decoction, is composed of Xia ku cao (*P. vulgaris*) and another three herbs, which has traditionally been used for softening hard lumps and resolving hard tissue masses [14]. Zhao J et al. reported that chemotherapy using *P. vulgaris* and taxane could improve the therapeutic effects of breast cancer and reduce its side effects [15]. *P. vulgaris* polysaccharide can inhibit human breast carcinoma-associated fibroblasts by inhibiting the expression of basic fibroblast growth factor and the growth of breast cancer cells [16]. The anti-proliferative activity of *P. vulgaris* polysaccharide (2.0 mg/mL) on the growth of human breast cancer MCF-7 cells was 31.8% [17]. In addition, some studies have demonstrated that 19α-hydroxy ursolic acid and quercetin present in *P. vulgaris* ethanol extract can inhibit the migration of tumour cells MDA-MB-231 in a dose dependent manner, in which quercetin reduces the proliferation of tumour cells by inhibiting the PI3k/Akt pathway. IC50 of 19α-hydroxy ursolic acid and quercetin against MDA-MB-231 cells migration was 1.676 μmol L^{-1} and 1.145 μmol L^{-1}, respectively [18]. The methanolic root extract of *P. vulgaris* was shown to exert potent anticancer effects in MCF-5 breast cancer cells both *in vitro* and *in vivo*, accompanied with apoptosis induction, inhibition of angiogenesis, cell cycle arrest, and modulation of PI3K/AKT signaling pathway [19]. In addition, because estrogen signaling is crucial for breast cancer cell growth, strategies designed to suppress estrogen signaling have been used to treat breast cancer patients. A recent study demonstrated *P. vulgaris* extracts exhibit anti-estrogenic effects *in vitro* and *in vivo*, and can be used as therapeutic agents for treatment of estrogen-dependent tumours [20]. In summary, *P. vulgaris* is a traditional Chinese medicine that has research prospects for antitumor and adjuvant treatment of breast cancer. However, to date, research on the anti-TNBC activity and mechanism of *P. vulgaris in vivo* is relatively scarce.

In this study, D101 macroporous resin was used to separate and prepare different fractions of the water extract from *P. vulgaris*. A 4T1-BALB/c transplanted breast cancer mouse model and three breast cancer cell models, including two TNBC cell models were used to screen the active groups of *P. vulgaris* against breast cancer. These results are expected to improve current clinical limitations regarding the unclear material basis of *P. vulgaris* on breast cancer and provide a new treatment strategy for TNBC.

2. Materials and methods

2.1. Plant materials

P. vulgaris was purchased from the Gaoqiao Medicinal Material Market (Changsha, Hunan Province, China). The origin of the herbal medicine was identified and authenticated by Professor Tasi Liu of Hunan University of Chinese Medicine.

2.2. Preparation of crude extract (PVE) and fractions from P. vulgaris

The *P. vulgaris* materials were ground into powder (60–80 mesh) and extracted (1 h each, 3 times) with boiling water (m: v = 1:10). Extracts were filtered and then combined and concentrated under reduced pressure to obtain *P. vulgaris* water extract (PVE).

Referring to the instruction manual, after pretreatment of D101 Macropore Adsorption resin (batch number HG 2-885-76, purchased from Tianjin Guangfu Fine Chemical Research Institute), PVE was sequentially eluted in water, 20%, 50% and 95% ethanol solutions. The flow rate was approximately 60 mL/min, and each gradient concentration elution was 5–6 times the column volume. After concentrating under reduced pressure, the eluted components were prefrozen at -20 °C for 24 h and then freeze-dried to obtain a powder of water eluted fraction (PVW), 20% ethanol eluted fraction (PV20), 50% ethanol eluted fraction (PV50) and 95% ethanol eluted component (PV95). The yield of each component was calculated.

2.3. High-performance liquid chromatography (HPLC) and ultraperformance liquid chromatography/tandem mass spectrometry (UPLC-MS/MS) analysis

Each fraction was reconstituted with 10 mL methanol (chromatographically pure), and 1 mL of which was taken, filtered through a 0.22 μmol/L microporous membrane, and used for liquid phase analysis. The reconstituted solution was diluted separately 5 times and centrifuged at 12,000 xg for 10 min at low temperature, and 800 μL of the supernatant was used for liquid quality analysis.

1 mg of rosmarinic acid, salviaflaside, luteolin (B20888, 98% purity, purchased from Shanghai Yuanye Biotechnology Co., Ltd.), ursolic acid (B21403, 98% purity, purchased from Shanghai Yuanye Biotechnology Co., Ltd.) and oleanolic acid (B20954, 98% purity, purchased from Shanghai Yuanye Biotechnology Co., Ltd.) standard was accurately weighed separately and dissolved with 1 mL methanol. Take 0.2 mL of rosmarinic acid (95% purity, laboratory-made), salviaflaside (95% purity, laboratory-made), and luteolin solution were mixed and diluted 10 times to prepare a mixed standard solution. Ursolic acid and oleanolic acid solutions (0.2 mL) were diluted 10 times to prepare oleanolic acid standard and ursolic acid standard, respectively.

A Waters e2695 HPLC (column: Agilent ZORBAX SB-C18, 4.6 × 250 mm, 5 μm) was used for preliminary analysis of PVE, PVW, PV20 and PV50 and mixed standard. The column temperature was 30 °C, and the injection volume was 5 μL. The wavelength was 256 nm. A 0.1% formic acid aqueous solution constituted mobile phase A, and acetonitrile was mobile phase B. The specific gradient elution conditions are shown in Table 1.

A Waters Acquity UPLC (column: Waters ACQUITY UPLC@BEH-C18, 2.1 mm × 50 mm, 1.7 μm) was used for preliminary analysis of PV95, oleanolic acid standard and the ursolic acid standard. The column temperature was 30 °C, the injection volume was 5 μL, and the wavelength was 210 nm. A 0.1% formic acid aqueous solution was used as mobile phase A, and acetonitrile was used as mobile phase B. The specific gradient elution conditions are shown in Table 2.

UHPLC-H-CLASS/XEVO G2-XS Qtof was used to preliminarily identify the components of *P. vulgaris*. The liquid phase conditions were as follows: 0.1% formic acid aqueous solution as mobile phase A, acetonitrile as mobile phase B, and gradient elution (0.00–4.00 min, 5.0%-20% B; 4.00–8.00 min, 20%-30%B; 8.00–15.00 min, 30%-50%B; 15.00–20.00 min, 50%-85%B; 20–22 min, 85%-100%B; 22–24 min, 100%-100%B; 24.00–28.00 min, 100%-5.0%B). The flow rate was 0.3 mL/min, the column temperature was 30 °C, and the injection volume was 5 μL. The mass spectrum conditions were as follows: ionization mode ES-, capillary (kV): 2.500; sampling cone: 40.000; source temperature (°C): 100; desolvation temperature (°C): 400; mass range: 100–1500 Da; cone gas flow (L/Hr): 50.0; and desolvation gas flow (L/Hr): 800.0. Preliminary structure determination was carried out by primary and multi-stage mass spectrometry.

Table 1. HPLC gradient elution conditions.

Time (min)	Flow (mL/min)	A%	B%
Initial	1.00	95.00	5.00
30	1.00	0.00	100.00

Table 2. UPLC gradient elution conditions.

Time	Flow (mL/min)	A%	B%
Initial	0.3	5	95
5	0.3	50	50
15	0.3	90	10
20	0.3	100	0
24	0.3	100	0

2.4. Cell lines and cell culture

Breast cancer cell lines MDA-MB-231, MCF-7 and 4T1 were purchased from the Shanghai Cell Bank located in the Chinese Academy of Science (Shanghai, China). MDA-MB-231 cells were cultured in DMEM high glucose complete medium, containing 10% foetal bovine serum and 1% penicillin-streptomycin. MCF-7 and 4T1 cells were cultured using RPMI 1640 complete medium containing 10% foetal bovine serum and 1% penicillin-streptomycin. Cells were cultured under conditions of 5% CO_2 at 37 °C.

2.5. Cell viability assay

The cell proliferation activity was detected by the MTT method [21]. Cells in the logarithmic growth phase (1×10^6/mL) were seeded in a 96-well culture plate (Beaver, 40196) with 100 μL per well at 37 °C for 24 h. Then, the cells were treated with drugs of gradient concentration for another 24–96 h. Subsequently, 100 μL MTT (0.5 mg mL^{-1}) was added to each well. Cultures were allowed to grow for an additional 4 h before DMSO (150 μL) was added. The relative cell viability was calculated by measuring the absorbance of each well in a microplate reader at 490 nm, and the experiments were repeated three times. The cell survival rate in response to drug treatments and to determine the concentration of drug that inhibited cell growth by 50% (IC_{50})was calculated.

2.6. Colony formation assay

Colony formation assay was performed according to a previously described method [22]. 4T1 cells in the logarithmic growth phase were inoculated into 6-well plates (1.2×10^3 cells/well). After culturing overnight, PV50 solutions of 62.5 μg mL^{-1}, 125 μg mL^{-1}, 250 μg mL^{-1}, 500 μg mL^{-1} and 1000 μg mL^{-1} were added to the cells as the drug group, complete medium was added as the control group, and cells were treated for 7–10 days. Then, cells were washed twice by precooled PBS, fixed with 4% paraformaldehyde solution at 4 °C for 1 h, stained with 0.5% crystal violet solution for 15 min, and washed with PBS again. The inhibition rate of clone formation was calculated according to the colony (>50 cells) under the microscope. The experiment was repeated 3 times.

2.7. Hoechst 33342 staining

The effect of PV50 on cell morphology was observed using Hoechst 33342 staining [23]. 4T1 cells in the logarithmic growth phase were seeded in 24-well plates (1.0×10^5 cells/well), then treated with different formulations of PV50 (62.5 μg mL^{-1}, 125 μg mL^{-1}, 250 μg mL^{-1}, 500 μg mL^{-1} and 1000 μg mL^{-1}) for 48 h. Then, the cells were washed with PBS and stained with Hoechst 33342 staining solution (10 μg/mL) for 25 min. Finally, stained cells were washed twice with PBS, and visualized using a fluorescence microscopy (Olympus IX-70, Olympus, Japan).

2.8. Determination of cell apoptosis by double staining with annexin V and PI

4T1 cells in the logarithmic growth phase were plated in 6-well plates (1.0×10^6 cells/well) and treated with continuous concentrations of PV50 (62.5, 125, 250, 500 and 1000 μg mL^{-1}) for 48 h. Then, cells were harvested and washed twice with PBS. Cells were resuspended in binding buffer (1×), and cell concentration was adjusted to 1.0×10^6/100 μL/test. Five microlitres of Annexin V and 10 μL of PI were added to each tube, vortexed gently to mix, and incubated for 15 min at room temperature in the dark. After staining, flow cytometry was used to assess apoptosis [24].

2.9. Flow cytometry to detect the effect of PV50 on the cell cycle

Cells were collected, adjusted to a cell density of 1.0×10^6/25 cm^2, and cultured for 24 h. After the cells became adherent, serum-free medium was added for 24 h. The control or PV50 (125, 250 and 500 μg mL^{-1}) was added and incubated for 48 h. Cells treated with different concentrations of drugs were digested and collected, centrifuged (1000 r·min^{-1}, 5 min) and washed twice with PBS. 200 μL of PBS was added to resuspend the cells and 750 μL of precooled absolute ethanol was slowly added dropwise until the concentration of ethanol solution was 75%. The cells were fixed and placed at 4 °C for 2 h. After centrifugation, ethanol was discarded, and cells were washed three times with PBS. Then, 100 μL of the prepared PI staining reagent was added, mixed, and stained in the dark at 37 °C for 30 min. After staining the cells, flow cytometry was used to detect the proportion of cells in each phase.

2.10. Cell scratched assay

Cell scratched assay was carried out according to the procedure as described by Razak et al. [25]. 4T1 cells (5×10^5/well) in the logarithmic growth phase were seeded into 12-well plates. When the cells grew close to confluence, a 20 μL pipette was used to draw three scratches in each well. The floating cells in the upper layer were removed by washing twice with PBS. Fresh medium with or without PV50 (125, 250 and 500 μg mL^{-1}) was added afterwards. An inverted microscope was used to observe cell morphology and take pictures at 12 h, 24 h and 48 h. ImageJ was used for data analysis. The experiment was repeated 3 times.

2.11. Animal model establishment of orthotopic transplantation for 4T1 breast cancer [26]

Animal experiments were conducted in accordance with the Guidelines for Animal Experimentation of Hunan University of Chinese Medicine (Changsha, China). Specific pathogen free (SPF) grade female BALB/c mice (5 weeks old, 18.13 ± 0.37 g) were purchased from Slack Jingda Experimental Animal Co., Ltd. (Changsha, China).

Prior to harvesting, 4T1 cells were grown in a 75 cm^2 cell culture flask (Beaver, 40175). When they reached 90% confluence, cells were trypsinized, harvested, rinsed and then suspended in PBS at a cellular concentration of 7×10^6/mL. Cells were collected within 1 h before modelling.

Experiment 1. After 60 female BALB/c mice (5 weeks old) were adaptively fed for one week, 50 of them were subcutaneously injected with PBS 4T1 cells (7×10^5) at the second pair of left breast pads, and the remaining 10 constituted the normal control group (NC) without any tumour induction. On the 7th day after inoculation with 4T1 cells, the modelled mice were randomly divided into the tumour control (TC, 0.2 mL pure water), tamoxifen (Tam, 5 mg kg^{-1}), PV20 (300 mg kg^{-1}), PV50 (300 mg kg^{-1}), PV95 (300 mg kg^{-1}) and NC groups were subjected intragastric administration for 21 days to screen the effective components from *P. vulgaris* against breast cancer *in vivo*.

Experiment 2. 60 female BALB/c mice (5 weeks old) were adaptively fed for one week. Then, 50 of them were subcutaneously injected with PBS 4T1 cells (7×10^5) at the second pair of left breast pads, and the remaining 10 constituted the normal control group (NC) without any tumour induction. On the 7th day, the modelled mice were randomly divided into the tumour control (TC, 0.2 mL pure water), tamoxifen citrate tablet (Tam, 5 mg kg^{-1}), PV50 low-, medium- and high-dose

(PV50D, 150 mg kg^{-1}; PV50Z, 300 mg/kg; PV50G, 600 mg/kg), and NC (0.2 mL pure water) groups with intragastric administration for 21 days to evaluate the antitumour effect of PV50 on 4T1-BALB/c breast cancer mice.

The body weight and tumour volume were recorded every three days. Tumour size was measured with digital callipers. Tumour volume was calculated according to the following formula: Tumour volume (mm^3) = 0.5×length×$width^2$. At the end of experiment, tumours and corresponding organs (spleen, heart, liver, kidney and lung) were collected, weighed and processed for hematoxylin-eosin staining (200×). Tumour inhibition rate was calculated by formula: Tumour inhibition rate (%) = [(mean tumour weight of TC group-tumour weight of treated group)÷mean tumour weight of TC group]×100.

2.12. Apoptosis evaluation using TUNEL assay

TUNEL cell apoptosis in situ was used to detect the apoptosis of tumour samples. For the terminal deoxynucleotidyl transferase dUTP-mediated nick-end labelling (TUNEL) assay, a paraffin block was sectioned, dewaxed and hydrated. Then, sections were incubated with Protease K according to the TUNEL kit (batch number 7791-13-1, purchased from Roche) manufacturer's instructions. Subsequently, samples were incubated with apoptosis detection kit enzyme mix (manufacturers protocol) for 60 min at 37 °C in a humidified environment and then washed with PBS. TUNEL-positive nuclei (fragmented DNA) were fluoresced by bright green light at 460 nm. Finally, nuclei were stained with 4,6-diamidino-2-phenylindole (DAPI) and rinsed. Photomicrographs were obtained using a fluorescence microscope (400×) with blue light at 454 nm of the nuclei after adding the fluorescence quenching agent. Apoptotic index (AI) defined as the percentage (%) of apoptotic cells was calculated according to the formula: AI (% of apoptotic cells)=(The number of TUNEL-positive cells÷Total number of cells)×100 [27].

2.13. Immunohistochemistry

Immunohistochemical analysis of tumour tissues was performed to examine the antitumour activity and mechanism of PV50 *in vivo* [24]. Tumour tissue sections were stained with polyclonal rabbit antibody for pro-apoptotic cleaved-caspase 3 (Affinity Biosciences Cat# AF7022, RRID:AB_2835326), according to the manufacturer's instructions. Immunohistochemical analysis was performed on deparafinated and rehydrated tissue sections. 3% H_2O_2 was added to block the activity of endogenous peroxidase. After blocking the nonspecific sites, slides were incubated with primary antibody for cleaved caspase-3 (1:100) at 4 °C overnight. After rewarming, secondary and tertiary antibodies were added for incubation. After development with DAB, the slides were counterstained with haematoxylin, dehydrated and dried, mounted and imaged under an upright optical microscope (Nikon Eclipse E100, Nikon, Japan) at 400× magnification. ImageJ software (National Institute of Health, Bethesda, MD, United States) was used to count for the number of immune-positive cells (cells with expression of cleaved caspase-3), which was expressed as % of positively stained cells =(The number of positively stained cells÷Total number of cells)×100 [27].

2.14. Acute toxicity study [28]

Female BALB/c mice (33–37 days) were continuously administered 1000 mg kg^{-1} PV50 for 14 days. The morphology and behaviour of mice were observed to determine if there was any toxicity, and their body weight was recorded every three days, with the last body weight was measured on day 15.

2.15. Statistical analysis

Data from the *in vivo* experiments are expressed as the mean ± standard error of the mean (S.E.M.) and were analysed by one-way analysis of variance using SPSS version 21.0 software. A value of $p < 0.05$ was considered statistically significant. IC50 values of the samples were calculated using Origin version 8.0 software (OriginLab Corporation, Noethampton, UK). The inhibitory type and Ki value were analysed using GraphPad Prism 7.0 software (GraphPad Software, Inc., La Jolla, CA, USA).

3. Results and discussion

3.1. HPLC and UPLC-MS/MS analysis

Among the extracted fractions of PVE eluted with D101 large resin, the yield of PV20 was the highest at 4.55%, and the yield of PV95 was the lowest at 1.09% (Supplementary Table 1S).

The results of HPLC (Supplementary Fig. 1S and 2S) and UPLC-MS/MS (Supplementary Fig. 3S) analysis showed that D101 macroporous resin effectively separated and enriched various compounds in PVE and PVW. The components of PV20, PV50 and PV95 were rather inconsistent in that PVW was primarily enriched in large polar components, PV20 was primarily composed of salviaflaside (retention time of 7.03 min, [MH]-521.130) and rosmarinic acid isomers (retention time of 8.10–8.35 min), [MH]-359.077)-based phenolic acid compounds, and PV50 contained a small amount of rosmarinic acid and did not contain salviaflaside. According to the mass spectrum structure, there were no characteristic compounds but rather, multiple isomers and the same type of compounds, which were inferred to be flavonoids, moderately polar triterpenes, and a small amount of phenolic acid in PV50. PV95 was primarily enriched in polar triterpenoid components, such as ursolic acid and oleanolic acid.

3.2. Screening of the effective fractions from P. vulgaris against breast cancer in vitro

According to reports in the literature, the water extract and other components of *P. vulgaris* effectively inhibit the proliferation of a variety of tumour cell lines, such as the TPC-1 human thyroid cancer cells, SW579 human thyroid cancer cells and human colon carcinoma HT-29 cells [29, 30]. In the present study, three breast cancer cell lines, MDA-MB-231 (a human TNBC cell line), MCF-7 (an estrogen receptor-positive human breast cancer cell line), and 4T1 (a mouse TNBC cell line), were used to investigate the anti-cancer effects of PV crude extracts and fractions. The viability of the cells was observed at different concentrations for 24 h (Figure 1). Then, the 50% growth inhibition (IC50) was assessed (Supplementary Table 2S). As shown in Figure 1A and Figure 1B, PVE had a proliferation inhibitory effect on MDA-MB-231 cells in a given drug concentration range. The inhibitory effect of PVW on MDA-MB-231 cell proliferation was weak and promoted proliferation in the low concentration range. PV20 had the same effect as PVE, which had a certain proliferation inhibitory effect. PV50 had a strong inhibitory effect on MDA-MB-231 cell proliferation with an IC50 value of 330.66 ± 7.36 μg mL^{-1}. Among the crude extract and fractions, PV95 had the strongest inhibitory effect on the proliferation of MDA-MB-231 cells, with an IC50 value of 73.32 ± 7.45 μg mL^{-1}. For MCF-7 cells (Figure 1C and Figure 1D), PVE had a certain effect on the proliferation of MCF-7 cells. The PVW and PV20 components did not inhibit the proliferation of MCF-7 cells. PV50 had a significant inhibitory effect on the proliferation of MCF-7 cells with an IC50 value of 596.63 ± 11.28 μg mL^{-1}. Among the crude extract and fractions, PV95 had the strongest inhibitory effect on MCF-7 cell proliferation, with an IC50 value of 116.73 ± 6.83 μg mL^{-1}. For 4T1 cells (Figure 1E and Figure 1F), PVE, PVW and PV20 had no obvious proliferation inhibitory effects. PV50 had a better proliferation inhibitory effect, and PV95 had the strongest proliferation inhibitory effect in a dose-dependent manner among the crude extract and fractions. PV50 showed higher sensitivity to MDA-MB-231 and 4T1 cells than MCF-7.

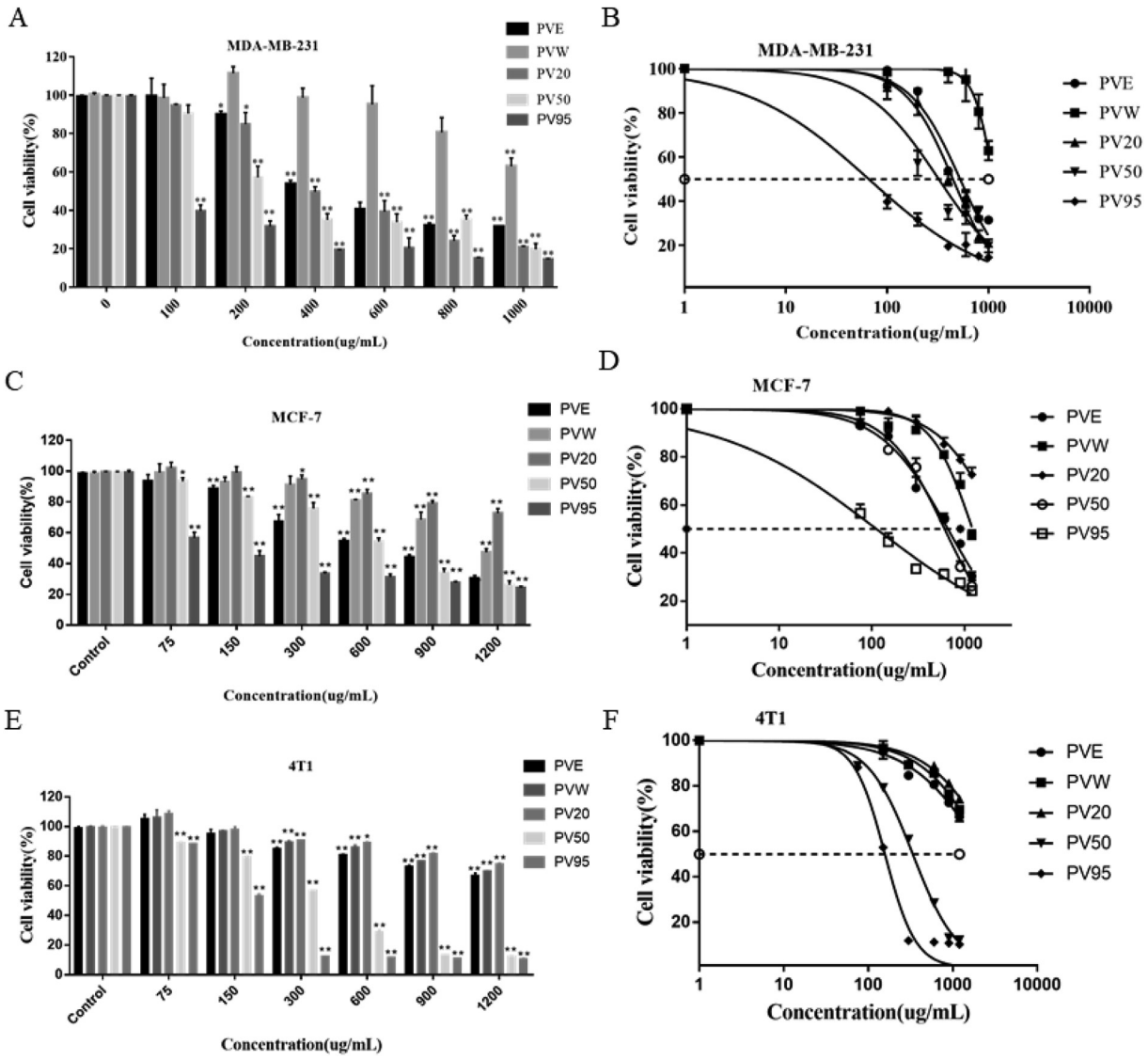

Figure 1. (A, C, E) The effects of PVE and fractions on the viability of MDA-MB-231, MCF-7 and 4T1 cells. (B, D, F) The intersections of each curve with the 50% dashed line correspond to the drug concentration (IC50) that yielded a survival rate of 50% (N = 3, $\bar{x} \pm s$; * and ** represent $p < 0.05$ and $p < 0.01$, respectively, compared to the control group).

3.3. Screening of the effective fractions from P. vulgaris against breast cancer in vivo

The mouse tumour bodies and tissue densities were similar, and the volume comparison could not be directly obtained by live CT scan. A homemade device (injector coil) was used to gently separate the tumour body from other parts. The size of the tumour could be intuitively compared under the left lens. The results showed (Figure 2A) that tumours in the TC group were the largest, and those in the Tam and PV50 groups were the smallest. In addition, through CT, complete bone could be seen without being affected.

The anti-breast cancer activity of each fraction of PV *in vivo* was evaluated by establishing 4T1 tumour-bearing mice. The tumour volume in the treatment groups were smaller than that in the control group (Fig. 2B and D). Tumours receiving treatment showed remarkable reduction of tumour weight, especially in the PV50 group (Figure 2C). The results showed that Tam (45.05 ± 0.06%), PV50 (62.42 ± 0.03%) and PV95 (41.13 ± 0.05%) effectively inhibited tumour growth, of which PV50 was the most effective (Supplementary Table 3S).

The Hematoxylin-eosin staining results (Figure 3A) indicated that tumour cells in the transplanted model group (TC) were arranged tightly, grew vigorously and showed cellular atypia, with large nuclei and clear nucleoli. After treatment, the tumour cells were arranged loosely, and necrotic cells were observed in the Tam, PV50 and PV95 groups. The formation of vacuoles often contributes to cell death, mainly due to the loss of membrane integrity and detachment from the substratum of cells [31, 32]. In the present study, compared with the model group, the number of vacuoles increased, while the number of tumour cells decreased to varying degrees in the Tam, PV50 and PV50 treatment groups, indicating that cancer cells had a certain degree of death. Figure 3B shows a section of normal mouse mammary glands. There was no significant difference on body weight of mice between groups (Figure 3C). After tumour transplantation, the spleens of mice were significantly swollen. Tam effectively reduced the ratio of spleen/body weight, and PV50 exhibited a tendency to decrease this parameter (Figure 3D). Figure 3E shows that in the spleen of the TC group, there was no complete white pulp structure and only a few red blood cells, but a large number of lymphocytes and more extramedullary haematopoietic cells were observed in the tissue. In the PV50 group, the red and white marrow boundaries were clearer, and the white marrow lymphocytes were slightly loosely arranged. A large number of red blood cells, more lymphocytes, and more extramedullary haematopoietic cells could be

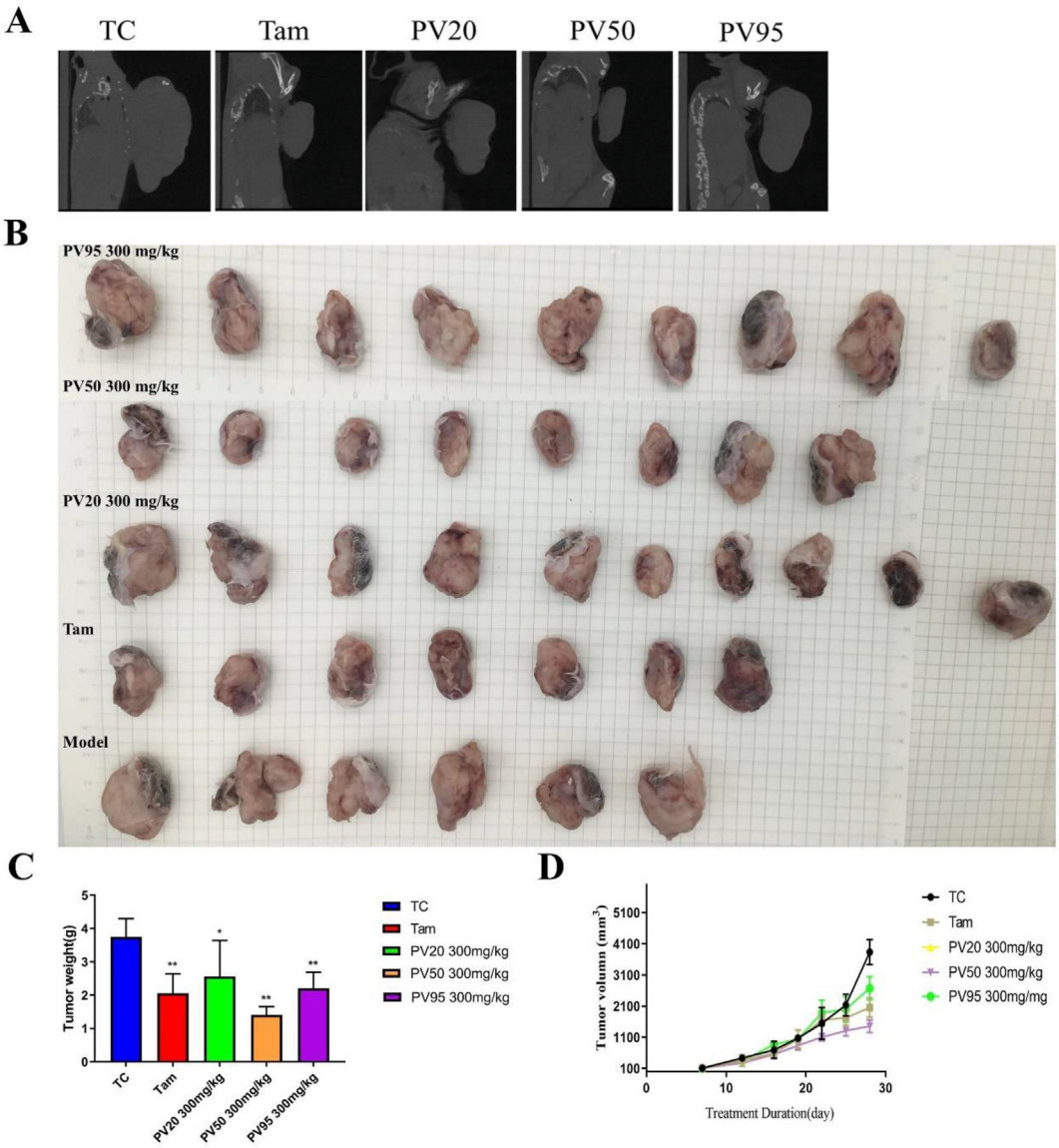

Figure 2. (A) Micro-CT scan of mouse tumours. (B) Visual diagram of isolated tumours in each group (n = 6–10). (C) Tumour weight (n = 6). (D) Tumour volume (n = 6). $*p < 0.05$, $**p < 0.01$ vs TC.

seen in the red pulp. The 4T1-transplanted breast cancer mouse model had highly metastatic characteristics. The tumour cells of lung tissues in the TC, PV20 and PV95 groups were active, and a large number of red blood cells appeared, while the tumour cells in the Tam group and PV50 group had less metastasis (Figure 3F). Furthermore, a large number of eosinophilic drop-like substances and a small amount of exfoliated bronchial epithelial cells were found in the bronchial lumen of the lung tissue of the NC group. In the TC group and other groups, the pulmonary structure was disordered, and the structure of the alveoli and alveolar wall was unclear. Tumour nodules appeared in the TC and PV95 groups. There was lymphocyte infiltration in PV50 vessel lumen.

In summary, compared with other fractions, PV95 and PV50 showed stronger inhibitory activity against three breast cancer cells, especially PV95. However, *in vivo* experiments, PV50 showed the best anti-breast cancer activity. Therefore, we subsequently selected PV50 to study the molecular mechanism of *P. vulgaris* against anti-breast cancer. The 4T1 mammary carcinoma is a transplantable tumour cell line originally isolated by Fred Miller and colleagues [33]. The 4T1 model is among the few murine TNBC models that spontaneously metastasize to sites affected in human breast cancer (eg, lung) in an immunocompetent host [34]. 4T1 cell line was selected for subsequent experiments in this study as it is a mouse TNBC cell line similar to that of human stage IV TNBC [34], and orthotopic transplantation of 4T1 cells offers a relevant tumour model to study efficacy of drug candidates or immune therapy regimens [35].

3.4. The effect of PV50 on the proliferation of 4T1 cells

MTT was used to determine the effect of PV50 on the proliferation activity of 4T1 cells. After treatment with different doses of PV50 for 24 h, 48 h and 72 h, PV50 inhibited 4T1 cells in a time- and dose-dependent manner compared to the control group (Figure 4A). The IC50 of PV50 on 4T1 proliferation at 24 h was 355.83 ± 22.16, 48 h was 272.17 ± 15.57, and 72 h was 200.53 ± 2.40 (Figure 4B). Combining plate cloning experiments to further verify the proliferation inhibitory activity of PV50 on 4T1 cells, the results showed that PV50 inhibited the formation of colonies of 4T1 cells in a dose-dependent manner (Figure 4C).

3.5. 4T1 cell apoptosis induced by PV50

The Hoechst 33342 staining method was used to observe cell morphology and to qualitatively analyse the effect of PV50 on 4T1 cells. As the dose of PV50 increased, 4T1 cells exhibited apoptotic

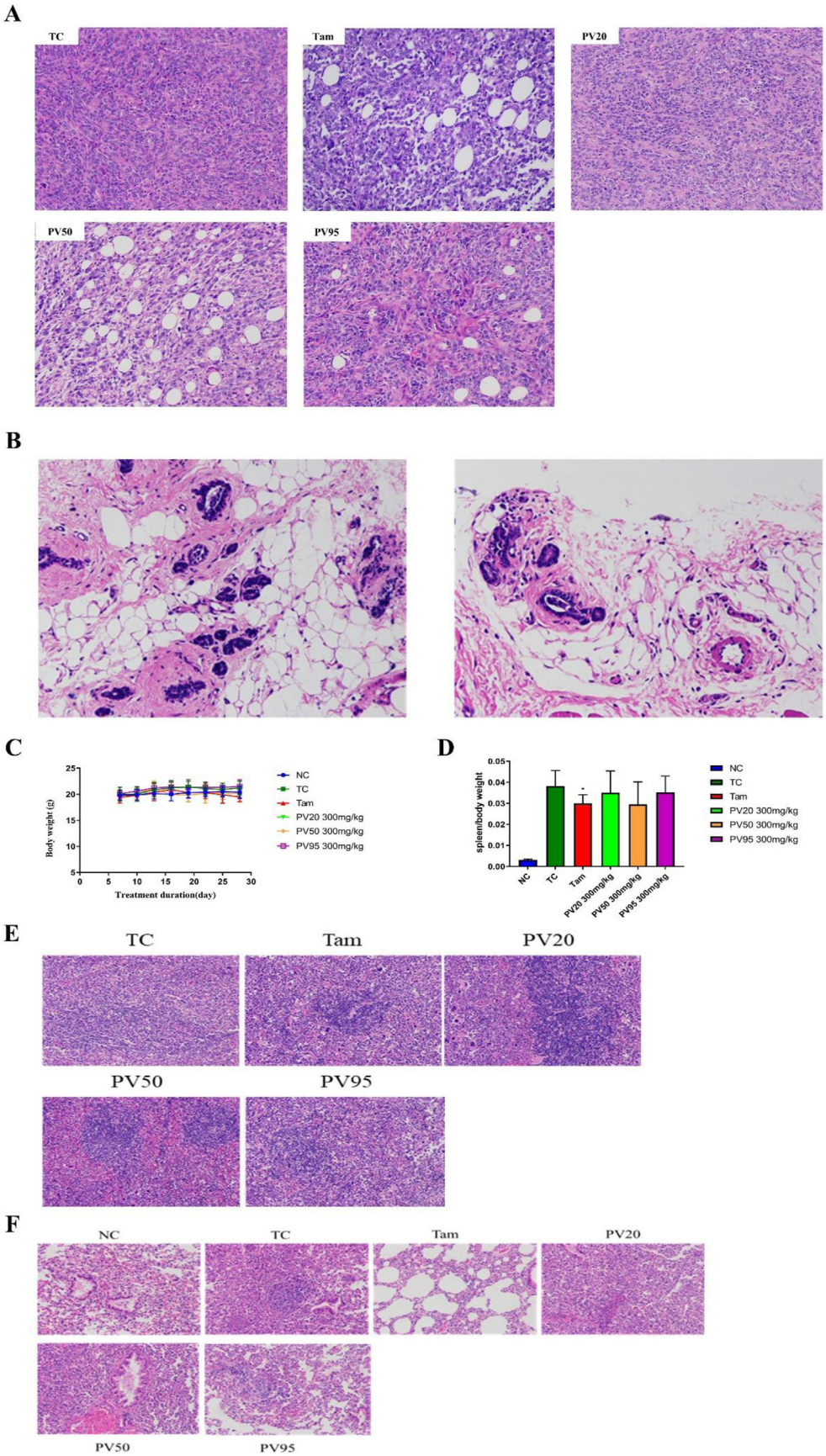

Figure 3. (A) Hematoxylin and eosin-stained sections of tumours treated with Tam and vary fractions (200×). (B) Hematoxylin-eosin staining of breast tissue in normal mice (200×). (C) Body weight of each group. (D) Spleen/weight ratio of each group. $*p < 0.05$, $**p < 0.01$ vs TC (n = 8–10). (E) Hematoxylin-eosin staining of spleen (200×). (F) Hematoxylin-eosin staining of lung (200×).

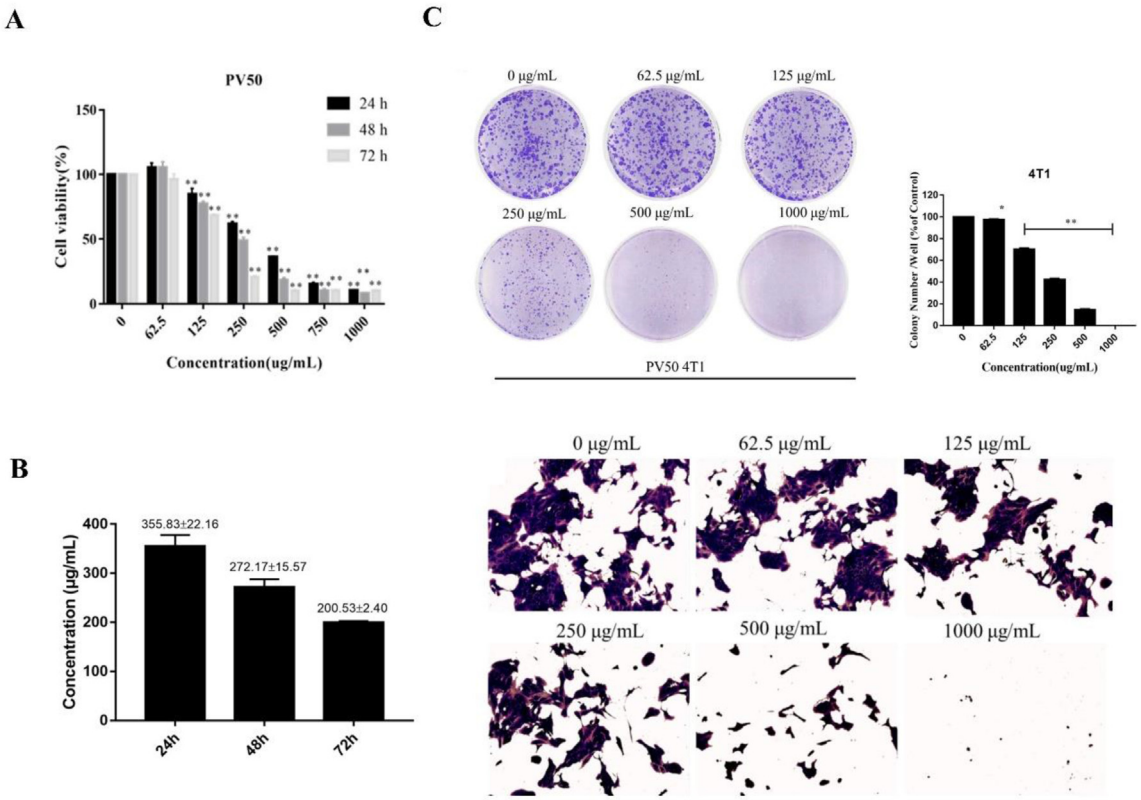

Figure 4. (A) The effects of different doses and different times on the proliferation activity of 4T1 cells (* and ** represent $p < 0.05$ and $p < 0.01$, respectively, compared to the control group). (B) The drug concentration with a survival rate of 50% (IC50) in 4T1 cells under different incubation times. (C) The effects of PV50 on 4T1 cell colony formation (* and ** represent $p < 0.05$ and $p < 0.01$, respectively, compared to the control group).

characteristics (Figure 5A), such as densely stained bright blue, concentrated or fragmented nuclei, and a reduced volume of nuclei. In the bright field, morphological changes, such as cell shrinkage, could be seen. After treatment with PV50 for 48 h, the apoptosis rates of cells was 2.61 ± 0.14%, 4.03 ± 0.63%, 6.7 ± 1.09%, 7.4 ± 1.52%, 12.84 ± 2.46%, and 33.61 ± 2.08% (Supplementary Table 4S), which increased with increasing doses of PV50 (Figure 5B).

3.6. The effect of PV50 on 4T1 cell cycle

PI staining and flow cytometry were used to detect the effect of PV50 on the 4T1 cell cycle. After 48 h of drug treatment of 4T1 cells, the G0/G1 phase increased with increasing doses of PV50 compared to the control group (Figure 5C). PV50 induced 4T1 cells to arrest in the G0/G1 phase (Figure 5D).

3.7. The effect of PV50 on cell migration

The cell scratch test was used to determine the effects of different concentrations of PV50 on cell migration at 12 h, 24 h and 48 h. The control group approached healing after 24 h. The results showed that healing of the scratches worsened and the migration area decreased with increasing concentrations of PV50 (Fig. 5E and F), indicating that PV50 exhibited a better inhibitory effect on cell migration activity.

3.8. The effect of PV50 on tumour size and tumour growth in 4T1 tumour-bearing mice

The tumour volume of mice was scanned by CT. As shown in Figure 6A, the tumour grew to the forelimb in the TC group, but with increasing doses of PV50, the tumour volume decreased. The bones of mice in each group were not significantly affected. Tumours receiving treatment showed remarkable reduction of tumour volume (Figure 6B and C) and tumour weight (Figure 6D) in the Tam and PV50G groups ($p < 0.05$). Histopathological analyses were carried out in the tumours for all experimental groups (Figure 6E). Tumour cells were grown with complete structure, compact arrangement and regular nuclei in TC group and PV50D group. After Tam, PV50Z or PV50G treatment, tumour cell necrosis, infiltration of inflammatory cells such as neutrophils and lymphocytes were observed. In addition, many tumour cells were swollen, the cytoplasm was loose or vacuolated, the nucleus was pyknotic, and a mass of karyorrhexis and karyolysis were noted. With increasing dose of PV50, tumour cell density was significantly reduced.

3.9. The effect of drugs on the body

The 4T1-BALB/c breast cancer mouse model exerted a good tumorigenesis effect. There was no death in mice with obvious palpable masses at 6–7 days. There was no significant difference in body weight between the treatment groups and the normal group (Figure 7A). After administration, mice were processed, and the various organs were measured. The results showed that there was no obvious difference between the hearts of each group, no obvious structural changes in the heart, and no obvious tumour metastasis (Figure 7C and Figure 7G). In addition, there were basically no obvious differences or pathological changes in the kidneys (Figure 7E and Figure 7G). Compared with the normal group, the liver of each group was enlarged with inflammatory cell infiltration, which may be related to the obstruction of hepatic venous return. The high-dose PV50 group exhibited reduced liver enlargement (Figure 7D and Figure 7G). The results of lung H-E staining showed that the structure of TC was disordered, the structure of alveolar and alveolar walls was unclear, a large number of tumour cells proliferated and grew, and a large number of inflammatory cells exuded. PV50D also showed a large amount of tumour cell proliferation and growth. The tissue structure of

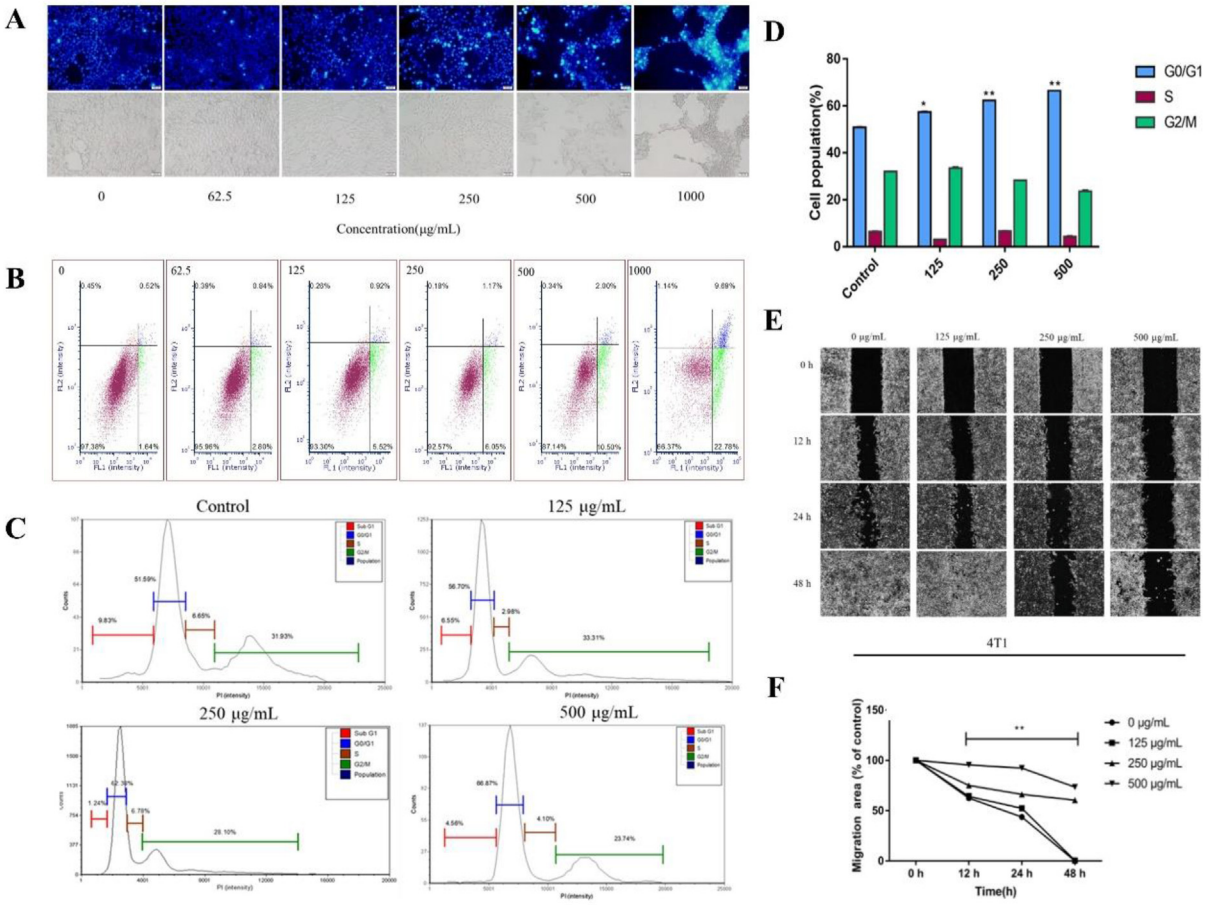

Figure 5. (A) Comparison of the morphological characteristics of 4T1 cell apoptosis induced by PV50 (Hoechst 33342 staining, 200×). (B) The effects on the apoptosis of PV50 (μg·mL^{-1}) on 4T1 cells. (C, D) The effects of PV50 on cell cycle in 4T1 cells (* and ** represent $p < 0.05$, $p < 0.01$, respectively, compared to the control group). (E, F) The effects of PV50 on scratch healing.

the positive drug group and high-dose PV50 group was not clear, but the metastasized number of tumour cells decreased (Figure 7F and Figure 7G). Generally, tumour bearing can lead to enlarged spleen and increased spleen index. Spleen enlargement is associated with increased cellularity. The accumulation of cells in the spleen provides cellular support for the spleen to exert immune regulation, which is associated with tumour immune escape. Some studies have shown that, the spleen is an immunological tissue that increases in size during various inflammatory challenges including infection and cancer, initiating an immune response directed towards specific tissues that need repair [36, 37]. Similar to Figure 3D, Tam and PV50G effectively reduced the spleen/-body mass index of tumour-bearing mice, and the degree of spleen lesions was effectively relieved (Figure 7B and Figure 7G). This may be related to the immune regulation played by Tam and PV50. The 4T1 tumour is highly metastatic, with lungs and liver as the principal target organs [38]. Additionally, 4T1 tumour can induce splenomegaly following orthotopic transplant into the mammary fatpads of female BALB/c mice [38].

3.10. The effect of PV50 on apoptosis of 4T1 breast cancer in BALB/c mice

When normal cells undergo apoptosis, their morphological characteristics gradually change. These changes include cell volume shrinkage, cytoplasmic shrinkage, dense nuclei, and chromosome shrinkage. Changes in cell morphology are the basis for determining whether apoptosis occurs [39]. Apoptosis was assessed by morphological changes in the cell nucleus after DAPI staining. DAPI dye can penetrate the complete cell membrane and then combine with the DNA double-stranded AT minor groove, showing uniform blue fluorescence. When a cell undergoes apoptosis, the permeability and integrity of the cell membrane are reduced, and the nucleus undergoes significant pyknosis. Therefore, the amount of DAPI in apoptotic cells increases, resulting in an increase in the bright blue fluorescent area in the cell. In addition, DNA fragmented by apoptosis produced a large amount of sticky end 3′-OH [40]. TUNEL staining can connect dUTP labelled with fluorescein and biotin to the 3′-OH end via terminal deoxynucleotidyl transferase. TUNEL-stained cells show strong green fluorescence spots, indicating DNA fragmentation [41].

TUNEL in situ cellular apoptosis experiments showed that after TUNEL staining, the TC group did not show green fluorescence, while the PV50 group and the positive drug group showed signs of green fluorescence, and the green fluorescence intensity of the PV50 group increased with increasing doses of PV50, indicating that PV50 and positive drugs induced tumour cells to produce DNA fragments (Figure 8A). Furthermore, as the concentration of PV50 increased, DNA fragmentation increased. The cell structure was complete and regular in the TC group. After treatment with PV50 and staining with DAPI, the cell structure was relatively complete in the PV50D group. Obvious apoptosis features [41] with cell morphological alterations, such as chromatin condensation, cell membrane blebbing, cell nucleus decomposition into fragments and many apoptotic bodies, were observed in cells treated with PV50Z. This

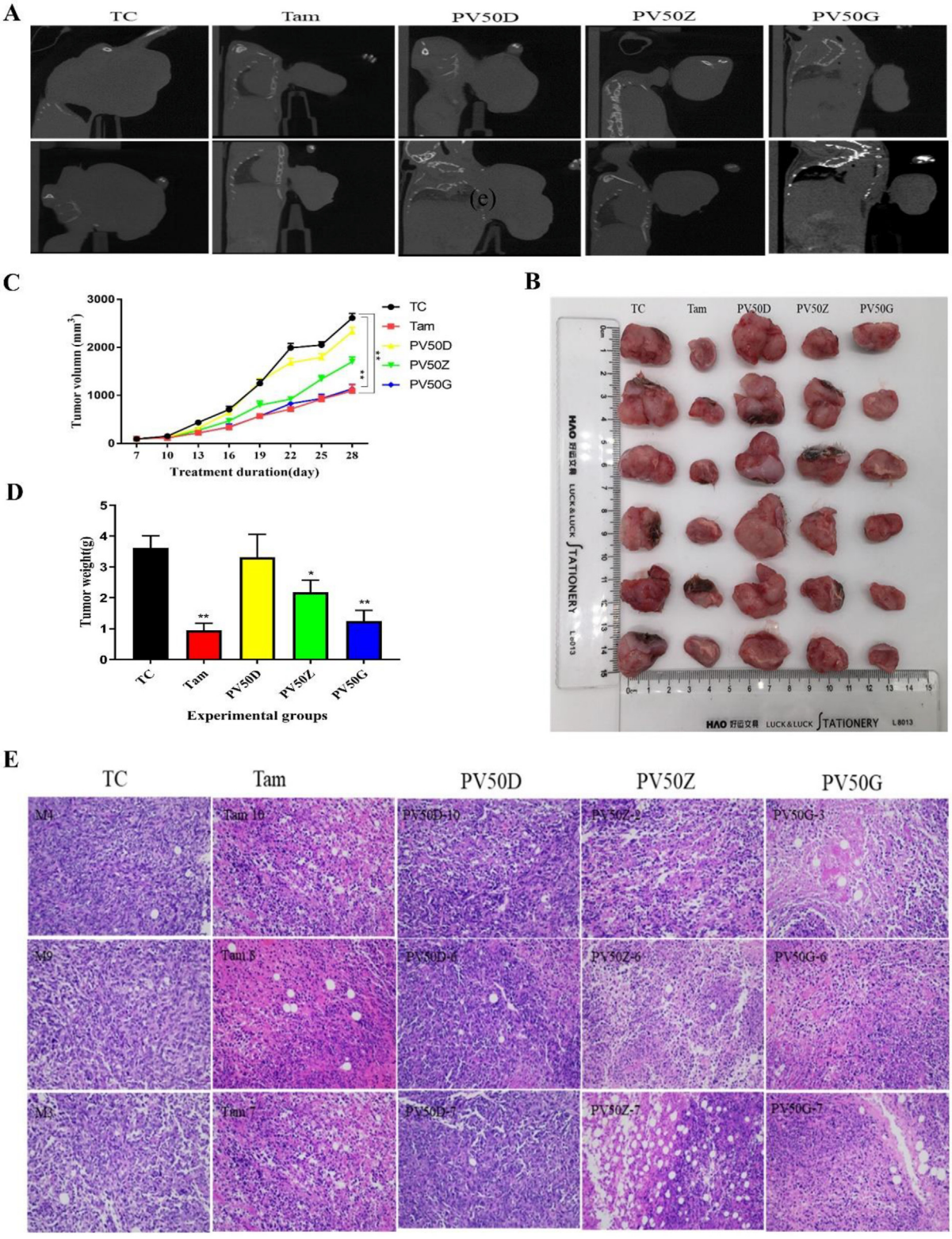

Figure 6. (A) Micro-CT scan of mouse tumours. (B) Visual diagram of isolated tumours in each group. (C) Tumour volume. *$p < 0.05$, **$p < 0.01$ vs TC (n = 8–10). (D) Tumour weight. *$p < 0.05$, **$p < 0.01$ vs TC (n = 8–10). (E) Effects of drugs on tumour pathological structure in tumour-bearing mice.

phenomenon was especially obvious after PV50G treatment, and the effect was even more significant than that of positive control drug (Figure 8C). In the overlapping image of TUNEL and DAPI staining, the specific green fluorescent position of TUNEL coincides with the chromatin condensation of DAPI staining and the fluorescent position of blue apoptotic bodies, indicating that PV50 induced DNA fragmentation and chromosome condensation. This shows that PV50 induces mouse 4T1 cell apoptosis by causing nuclear DNA loss.

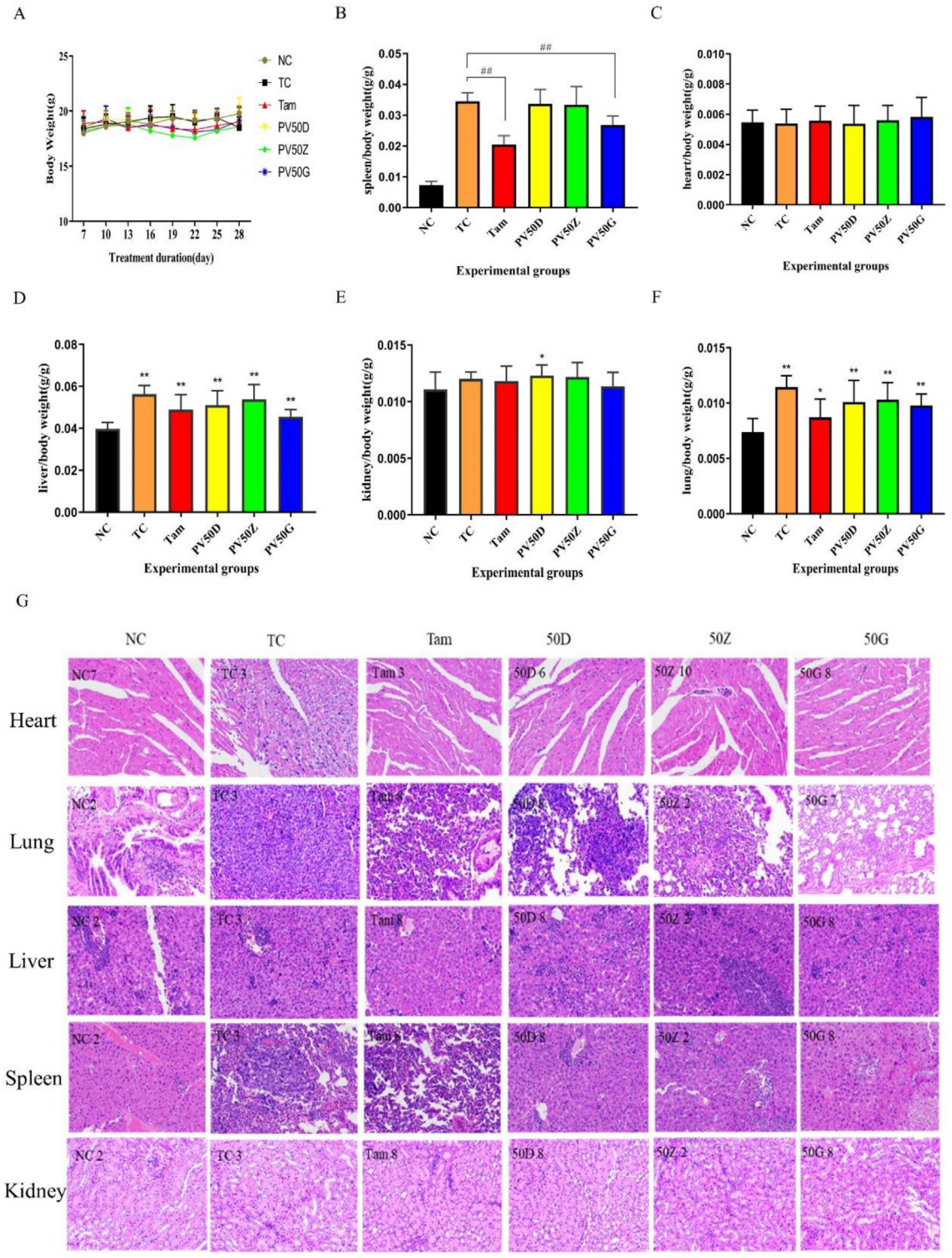

Figure 7. (A) The body weight of each group. (B) The ratio of spleen/body weight. Different marks within treatments indicate significant differences at $^{\#}p < 0.05$ and $^{\#\#}p < 0.01$ compared to the TC group (n = 10). (C) The ratio of heart/body weight. (D) The ratio of liver/body weight. (E) The ratio of kidney/body weight. (F) The ratio of lung/body weight. Different marks within treatments indicate significant differences at $^{*}p < 0.05$ and $^{**}p < 0.01$ compared to the NC group (n = 10). (G) Histopathological sections of mouse organs in each group (200×).

3.11. Immunohistochemistry

Apoptosis is widely recognized to play an important role in the inhibition and resistance of the development of tumours, which may be triggered by signals from within the cell [42]. It is widely accepted that loss of mitochondrial membrane potential can cause the release of a variety of proapoptotic signals, leading to the cell death [43]. The caspase enzymes contribute to the mitochondrial pathway's ability to regulate apoptosis [44]. Among them, caspase-3 is one of the key executioners of apoptosis [45].

In the present study, the paraffin-embedded tissue was labelled with cleaved caspase 3 antibody to observe the effects of PV50 on tumour cell

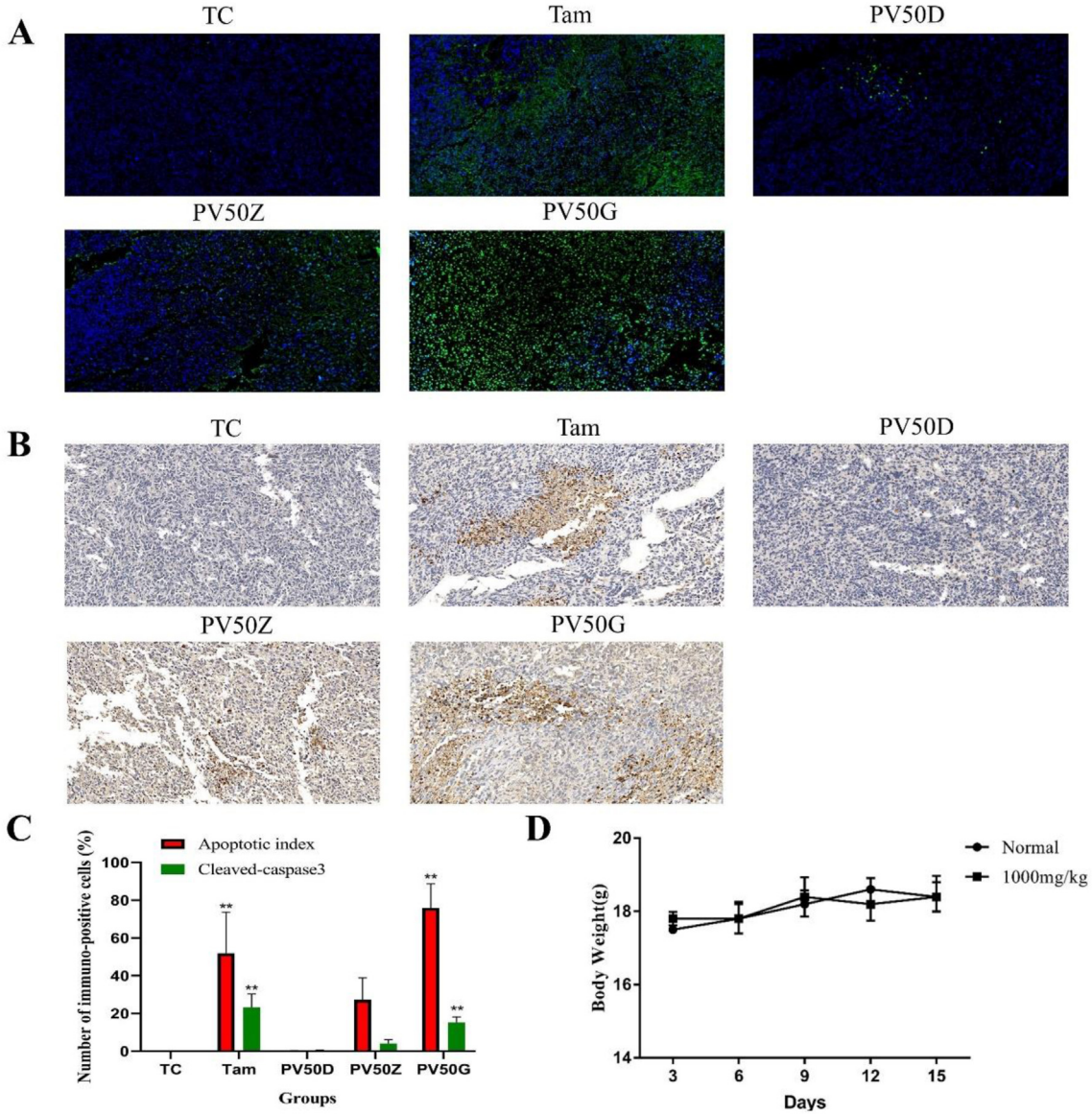

Figure 8. (A) The effects of drugs on tumour cell apoptosis. Green spots represent apoptotic bodies, and blue spots represent cell nuclei (400×). (B) The effects of drugs on the expression of cleaved caspase-3 in tumour tissue (400×). (C) Cleaved caspase 3 and corresponding frequencies of TUNEL positive cells expressed as AI. Different marks within treatments indicate significant differences at $*p < 0.05$ and $**p < 0.01$ compared to the TC group (n = 3). (D) Weight change trends in 10 acutely toxic experimental mice.

apoptosis. The results showed that cleaved caspase-3 was positive and stained brown (Figure 8B). Compared to the TC group, the expression rates of cleaved caspase-3 in the tissue increased as the PV50 dose increased (Figure 8C). This indicates that PV50 plays a role in promoting apoptosis, which may be related to cleaved caspase-3.

3.12. Acute toxicity study

Within 14 days of continuous feeding (1000 mg kg^{-1} PV50), the survival rate of mice was 100%. A gradual body weight increase was observed, but the changes were not significantly different compared with the normal group. No physical changes was observed in behavior patterns and fur of the mice (Figure 8D).

4. Discussion

There is increasing interest in herbal and botanical remedies in oncotherapy. *P. vulgaris*, a common plant cultured in China, Korea, Japan and Europe, has been established to have anti-inflammatory, anti-viral and anti-cancer activities [46, 47]. The traditional use of *P. vulgaris* is for the treatment of liver cancer in a few areas of China. At present, it is used primarily for the treatment of thyroid cancer, throat cancer, and lymphosarcoma among others [48].

In the present study, the anti-breast cancer activities of water extract and different ethanol-eluted fractions of *P. vulgaris* were compared both *in vivo* and *in vitro*, and PV50 was initially screened as the fraction with the best anti-breast cancer activity. Our results clearly depicts that PV50 significantly inhibited the proliferation of triple-negative breast tumour cells, induced cell apoptosis, regulated the cell cycle and inhibited tumour cell migration *in vitro*. *P. vulgaris* has been shown to induce cell cycle arrest at various checkpoints in cancer cells. PV50 induced 4T1 cells to arrest in the G0/G1 phase. According to the literature, after thyroid carcinoma cell line SW579 was treated with *P. vulgaris*, the proportion of cells in the G0/G1 phase was significantly increased when compared to the control group [49]. Ursolic acid from *P. vulgaris* could block B16 mouse melanoma cell line in G1 phase [50]. It suggest that *P. vulgaris* is

capable of inducing cell cycle arrest in various cancer cell lines. One of the key steps in successful breast cancer metastasis is cancer cell migration and invasion [51] Migrating cells can result in less sensitivity to apoptosis and standard chemotherapy [52]. Therefore, the strategy to preventing metastasis by targeting the elements that regulate the migratory and invasive capacities of cancer cells promises to reduce the spread of tumour cells [52]. The aqueous extract of *P. vulgaris* suppresses cell invasion and migration in human liver cancer cells by attenuating matrix metalloproteinases [52]. Rosmarinic acid, a major phenylpropanoid isolated from *P. vulgaris*, can significantly suppress cell viability, cell growth, cell invasion and migration as well as epithelial mesenchymal transition (EMT) of pancreatic cancer cells, and induce cell apoptosis in pancreatic cancer cells [53].

Ruanjian Sanjie (RJSJ) decoction, is composed of four herbs, including Ban xia (*Pinellia ternata*), Xia ku cao (*Prunella vulgaris*), Shan ci gu (*Cremastra appendiculata*) and Hai zao (Sargassum pallidum), and has traditionally been used for softening hard lumps and resolving hard tissue masses. RJSJ also shows potent cytotoxicity against breast cancer cells *in vitro* by the suppression of the anti-apoptotic proteins B-cell lymphoma 2 and survivin, leading to the activation of caspase-3/7 and caspase-9, and the apoptotic cascade [14]. Caspase-3 is an important apoptosis effector of the caspases family, and associated in inactivating many related proteins affecting cell structure, cell cycle and DNA repair finally leading to apoptosis [54].

The 4T1 breast cancer cells are easily transplanted into the mammary fat pad allowing for easy quantication of tumour growth and progression [55]. To further determine the activity of PV50 against triple-negative breast cancer, a 4T1 cell transplantation-BALB/c breast cancer mouse model was constructed. In the present study, it was found that PV50 medium and high dose groups could slow down tumour development and reduce tumour size, indicating that PV50 has anti-breast cancer activity *in vivo*. The H-E staining of the histopathological structure of breast cancer showed that the PV50 component at medium and high doses caused tumour cell necrosis, loss, and inflammatory cell infiltration. Abnormal tumour cells lead to apoptosis inhibition, and excessive cell proliferation, and apoptosis induction has been a hot target of tumour therapy [56]. Promoting apoptosis of breast cancer cells is also a hot topic in the study of anti-breast cancer. In order to discover the molecular mechanism of PV50 against breast cancer, apoptosis of tumour tissue was observed by TUNEL staining. The results showed that, PV50 inhibited tumour growth, inhibited lung metastasis, and induced cell apoptosis in BALB/c-transplanted tumour mice. With the increase of PV50 dose, the apoptosis of tumour cells was more significant. The mechanism may be related to induce damage of nuclear DNA and increase expression of cleaved caspase-3. In the transplanted tumour mice, there the spleen was markedly enlarged and dim after dissection. The giant spleen phenomenon in tumour-bearing mice is related to the accumulation of immunosuppressive cells MDSCs in the spleen. However, tamoxifen could reduce the effect of the giant spleen phenomenon in tumour-bearing mice. In additionspleens in the PV50 group were relatively close to normal, indicating that PV50 may also play a role in cancer immunity.

Analyzed by HPLC and UPLC-MS/MS, the PV50 was identified as flavonoids, moderately polar triterpenes, and a small amount of phenolic acid. It was also revealed that *P. vulgaris* may activating the caspase-3 cascade and inducing apoptosis [46]. The triterpenoid, flavonoids, and phenylpropanoids in *P. vulgaris* have shown a collective therapeutic effect against cancer mediated through multiple pathways [47]. Several phytochemicals from *P. vulgaris* including oleanic acid [57] and ursolic acid [58] have also been shown to either induce or promote apoptosis in cancer cells. Total flavonoids from *P. vulgaris* have an obvious anti-hepatocarcinoma effect, and the mechanism may be linked to the inhibition of autophagy and promotion of apoptosis in liver cancer cells [48].

5. Conclusion

In the present study, we first screened the best active fraction from the crude extract (PVE) and ethanol eluted fractions of *P. vulgaris* by using MDA-MB-231, MCF-7, 4T1 cell models *in vitro* and a 4T1-BALB/c transplanted tumour mouse breast cancer model *in vivo*. Furthermore, the anti-breast cancer mechanism of the best active fraction was investigated. The results demonstrated that PVE and ethanol fractions exhibited anti-breast cancer activity, especially with the 50% ethanol eluted fraction (PV50), which effectively regulated the 4T1 cell cycle, inhibited tumour cell proliferation, and promoted cancer cell apoptosis. In case of *in vivo* assays, PV50 inhibited tumour growth and lung metastasis, as well as inducing cell apoptosis by promoting damage of nuclear DNA and increasing expression of cleaved caspase-3. In addition, the chemical compositions of PV50 were analyzed by HPLC and UPLC-MS/MS, which were identified as flavonoids, moderately polar triterpenes, and a small amount of phenolic acid. The aqueous extract from *P. vulgaris* and its ethanol fractions could be applied as natural sources against breast cancer in the pharmaceutical industry. These findings provide a basis for understanding the mechanism of the anti-breast cancer activity of *P. vulgaris*.

Declarations

Author contribution statement

Hongshan Luo: Performed the experiments; Analyzed and interpreted the data.

Lingjia Zhao: Performed the experiments; Analyzed and interpreted the data; Wrote the paper.

Yamei Li: Performed the experiments.

Bohou Xia: Analyzed and interpreted the data.

Yan Lin; Jingchen Xie: Contributed reagents, materials, analysis tools or data.

Ping Wu: Conceived and designed the experiments.

Duanfang Liao; Limei Lin: Conceived and designed the experiments; Contributed reagents, materials, analysis tools or data.

Zhimin Zhang: Analyzed and interpreted the data; Wrote the paper.

Funding statement

Dr. Zhimin Zhang was supported by Project of Changsha Science and Technology Bureau [kq2004061], The Youth Natural Science Foundation of Hunan Province [2019JJ50449].

Yamei Li was supported by Hunan Province Traditional Chinese Medicine Research Program [2021056].

Limei Lin was supported by Hunan Province Science and Technology Innovation Leading Talent Project [2021RC4034], Key Project of Hunan Provincial Department of Education [20A380], Hunan Science and Technology Innovation Team Project [2021RC4064], First-class Discipline Project on Chinese Pharmacology of Hunan University of Chinese Medicine [201803].

Data availability statement

Data included in article/supp. material/referenced in article.

Declaration of interests statement

The authors declare no conflict of interest.

Additional information

Supplementary content related to this article has been published online at https://doi.org/10.1016/j.heliyon.2022.e11183.

References

[1] I. Cohen, M. Tagliaferri, D. Tripathy, Traditional Chinese medicine in the treatment of breast cancer, Semin. Oncol. 29 (2002) 563–574.

[2] M.S. Moran, Radiation therapy in the locoregional treatment of triple-negative breast cancer, Lancet Oncol. 16 (3) (2015) 113–122.

[3] Y.X. Feng, M. Spezia, S.F. Huang, C.F. Yuan, Z.Y. Zeng, L.H. Zhang, X.J. Ji, W. Liu, B. Huang, W.P. Luo, B. Liu, Y. Lei, S. Du, A. Vuppalapati, H. H Luu, R. C Haydon, T.C. He, G.S. Ren, Breast cancer development and progression: risk factors, cancer stem cells, signaling pathways, genomics, and molecular pathogenesis, Genes Dis 5 (2) (2018) 77–106.

[4] M. Tao, D.L. Ma, Y. Li, C. Zhou, Y. Li, Y.S. Zhang, W.M. Duan, X.J. Xu, R. Wang, L.Z. Wu, H.Y. Liu, Clinical significance of circulating tumor cells in breast cancer patients, Breast Cancer Res. Treat. 129 (1) (2011) 247–254.

[5] D.P. Kodack, V. Askoxylakis, G.B. Ferraro, D. Fukumura, R.K. Jain, Emerging strategies for treating brain metastases from breast cancer, Cancer Cell 27 (2) (2015) 163–175.

[6] A.S. Azmi, S.H. Bhat, S. Hanif, S.M. Hadi, Plant polyphenols mobilize endogenous copper in human peripheral lymphocytes leading to oxidative DNA breakage: a putative mechanism for anticancer properties, FEBS Lett. 580 (2) (2006) 533–538.

[7] J. Malíková, J. Swaczynová, Z. Kolář, M. Strnad, Anticancer and antiproliferative activity of natural brassinosteroids, Phytochemistry 69 (2) (2008) 418–426.

[8] M. Greenwell, P.K.S.M. Rahman, Medicinal plants: their use in anticancer treatment, Int. J. Pharma Sci. Res. 6 (10) (2015) 4103–4112.

[9] National Pharmacopoeia Commission, Pharmacopoeia of the People's Republic of China, Volume 1, China Medico-Pharmaceutical Science & Technology Puhlishig House, Beijing, 2020.

[10] Z.M. Zhang, Y.M. Zhou, Y. Lin, Y.M. Li, B.H. Xia, L.M. Lin, D.F. Liao, GC-MS-based metabolomics research on the anti-hyperlipidaemic activity of *Prunella vulgaris* L. polysaccharides, Int. J. Biol. Macromol. 159 (2020) 461–473.

[11] Y.B. Bai, B.H. Xia, W.J. Xie, Y.M. Zhou, J.C. Xie, H.Q. Li, D.F. Liao, L.M. Lin, C. Li, Phytochemistry and pharmacological activities of the genus *Prunella*, Food Chem. 204 (2016) 483–496.

[12] J. Tan, H. Qi, J. Ni, Extracts of endophytic fungus xkc-s03 from *Prunella vulgaris* L. spica inhibit gastric cancer *in vitro* and *in vivo*, Oncol. Lett. 9 (2) (2015) 945–949.

[13] Y.J. Hwang, E.J. Lee, H.R. Kim, K.A. Hwang, *In vitro* antioxidant and anticancer effects of solvent fractions from *Prunella vulgaris* var. lilacina, BMC Compl. Alternative Med. 13 (2013) 310.

[14] X.M. Zhao, J. Zhao, R.J. Hu, Q. Yao, G.X. Zhang, H.S. Shen, E. Yagüe, Y.H. Hu, Ruanjian Sanjie decoction exhibits antitumor activity by inducing cell apoptosis in breast cancer, Oncol. Lett. 13 (5) (2017) 3071–3079.

[15] J. Zhao, D. Ji, X. Zhai, L. Zhang, X. Luo, X. Fu, Oral administration of *Prunella vulgaris* L improves the effect of taxane on preventing the progression of breast cancer and reduces its side effects, Front. Pharmacol. 9 (2018) 806.

[16] J. Hao, X.L. Ding, X. Yang, X.Z. Wu, *Prunella vulgaris* polysaccharide inhibits growth and migration of breast carcinoma-associated fibroblasts by suppressing expression of basic fibroblast growth factor, Chin. J. Integr. Med. 26 (4) (2020) 270–276.

[17] C. Li, X. Fu, Q. Huang, F. Luo, L. You, Ultrasonic extraction and structural identification of polysaccharides from *Prunella vulgaris* and its antioxidant and antiproliferative activities, Eur. Food Res. Technol. 240 (1) (2015) 49–60.

[18] Y.B. Bai, C. Li, Y.M. Zhou, S.L. Pi, B.H. Xia, Chemical constituents of triterpenoids from *Prunella vulgaris* and their antitumor activities, Chin. Tradit. Herb. Drugs 46 (2015) 3623–3629.

[19] W. Gao, HLYLYLY Xu, Root extract of *Prunella vulgaris* inhibits *in vitro* and *in vivo* carcinogenesis in MCF-5 human breast carcinoma via suppression of angiogenesis, induction of apoptosis, cell cycle arrest and modulation of PI3K/AKT signalling pathway, J. BUON. 24 (2) (2019) 549–554.

[20] N. H Collins, E. C Lessey, C. D DuSell, D. P McDonnell, L. Fowler, W.A. Palomino, M. J Illera, X.Z. Yu, B. Mo, A. M Houwing, B.A. Lessey, Characterization of antiestrogenic activity of the Chinese herb, *Prunella vulgaris*, using *in vitro* and *in vivo* (Mouse Xenograft) models, Biol. Reprod. 80 (2) (2009) 375–383.

[21] J.Y. Park, Y.W. Kwon, S.C. Lee, S.D. Park, J.H. Lee, Herbal formula SC-E1 suppresses lipopolysaccharide-stimulated inflammatory responses through activation of Nrf2/HO-1 signaling pathway in RAW 264.7 macrophages, BMC Compl. Alternative Med. 17 (1) (2017) 374.

[22] S. Yang, J. Chen, T. Tan, N. Wang, Y. Huang, Y. Wang, X. Yuan, P. Zhang, J. Luo, X. Luo, Evodiamine exerts anticancer effects against 143B and MG63 cells through the Wnt/β-catenin signaling pathway, Cancer Manag. Res. 12 (2020) 2875–2888.

[23] P. Wu, Q. Zhou, H. Zhu, Y. Zhuang, J. Bao, Enhanced antitumor efficacy in colon cancer using EGF functionalized PLGA nanoparticles loaded with 5-Fluorouracil and perfluorocarbon, BMC Cancer 20 (1) (2020) 354.

[24] H. Li, Y. Qian, X. Wang, R. Pi, X. Zhao, X. Wei, Targeted activation of Stat3 in combination with paclitaxel results in increased apoptosis in epithelial ovarian cancer cells and a reduced tumour burden, Cell Prolif 53 (1) (2020), e12719.

[25] N.A. Razak, N. Abu, W.Y. Ho, N.R. Zamberi, S.W. Tan, N.B. Alitheen, K. Long, S.K. Yeap, Cytotoxicity of eupatorin in MCF-7 and MDA-MB-231 human breast cancer cells via cell cycle arrest, anti-angiogenesis and induction of apoptosis, Sci. Rep. 9 (1) (2019) 1514.

[26] S. Sun, K. Li, Z. Lei, L. Xiao, R. Gao, Z. Zhang, Immunomodulatory activity of polysaccharide from Helicteres angustifolia L. on 4T1 tumor-bearing mice, Biomed. Pharmacother. 101 (2018) 881–888.

[27] L. Nežić, L. Amidžić, R. Škrbić, R. Gajanin, E. Nepovimova, M. Vališ, K. Kuča, V. Jaćević, Simvastatin inhibits endotoxin-induced apoptosis in liver and spleen through up-regulation of survivin/NF-κB/p65 expression, Front. Pharmacol. 10 (2019) 54.

[28] M. Paydar, B. Kamalidehghan, Y.L. Wong, W.F. Wong, C.Y. Looi, M.R. Mustafa, Evaluation of cytotoxic and chemotherapeutic properties of boldine in breast cancer using in vitro and in vivo models, Drug Des. Dev. Ther. 8 (2014) 719–733.

[29] F.Q. Yu, L.L. Zhang, R.S. Ma, C.G. Liu, Q.D. Wang, D.T. Yin, The antitumour effect of *Prunella vulgaris* extract on thyroid cancer cells in vitro and in vivo, Evid Based. Compl. Alternat. Med. (2021), 8869323.

[30] W. Lin, L.P. Zheng, Q.C. Zhuang, A.L. Shen, L.Y. Liu, Y.Q. Chen, T. J Sferra, J. Peng, *Spica Prunellae* extract inhibits the proliferation of human colon carcinoma cells via the regulation of the cell cycle, Oncol. Lett. 6 (4) (2013) 1123–1127.

[31] A.V. Shubin, I.V. Demidyuk, A.A. Komissarov, L.M. Rafieva, S.V. Kostrov, Cytoplasmic vacuolization in cell death and survival, Oncotarget 7 (34) (2016) 55863–55889.

[32] D. Wang, R. Huo, C. Cui, Q. Gao, J. Zong, Y. Wang, Y. Sun, R. Hou, Anticancer activity and mechanism of total saponins from the residual seed cake of Camellia oleifera Abel. in hepatoma-22 tumor-bearing mice, Food Funct. 10 (5) (2019) 2480–2490.

[33] B.A. Pulaski, S. Ostrand-Rosenberg, Mouse 4T1 breast tumor model. *Current protocols in immunology*, *Chapter 20*, Curr. Protoc. Im. (2001).

[34] K. Tao, M. Fang, J. Alroy, G.G. Sahagian, Imagable 4T1 model for the study of late stage breast cancer, BMC Cancer 8 (2008) 228.

[35] P. Lasso, M. Llano Murcia, T.A. Sandoval, C. Urueña, A. Barreto, S. Fiorentino, Breast tumor cells highly resistant to drugs are controlled only by the immune response induced in an immunocompetent mouse model, Integr. Cancer Ther. 18 (2019), 1534735419848047.

[36] E.A. Murphy, J.M. Davis, T.L. Barrilleaux, J.L. McClellan, J.L. Steiner, M.D. Carmichael, M.M. Pena, J.R. Hebert, J.E. Green, Benefits of exercise training on breast cancer progression and inflammation in C3(1)SV40Tag mice, Cytokine 55 (2) (2011) 274–279.

[37] J.Á. Balog, L. Jr Hackler, A.K. Kovács, P. Neuperger, R. Alföldi, L.I. Nagy, L.G. Puskás, G.J. Szebeni, Single cell mass cytometry revealed the immunomodulatory effect of cisplatin via downregulation of splenic CD44+, IL-17A + MDSCs and promotion of circulating IFN-γ+ Myeloid cells in the 4T1 metastatic breast cancer model, Int. J. Mol. Sci. 21 (1) (2019) 170.

[38] S.A. DuPré, D. Redelman, K.W. Jr Hunter, The mouse mammary carcinoma 4T1: characterization of the cellular landscape of primary tumours and metastatic tumour foci, Int. J. Exp. Pathol. 88 (5) (2007) 351–360.

[39] C. Bortner, J. Cidlowski, A necessary role for cell shrinkage in apoptosis, Biochem. Pharmacol. 56 (12) (1998) 1549–1559.

[40] D. Loo, In situ detection of apoptosis by the TUNEL assay: an overview of techniques, Methods Mol. Biol. 682 (2011) 3–13.

[41] T. Wu, X. Duan, C. Hu, C. Wu, X. Chen, J. Huang, et al., Synthesis and characterization of gold nanoparticles from Abies spectabilis extract and its anticancer activity on bladder cancer T24 cells, Artif. Cell Nanomed. Biotechnol. 47 (1) (2019) 512–523.

[42] R.S. Wong, Apoptosis in cancer: from pathogenesis to treatment, J. Exp. Clin. Cancer Res. 30 (1) (2011) 1–14.

[43] G. Kroemer, L. Galluzzi, C. Brenner, Mitochondrial membrane permeabilization in cell death, Physiol. Rev. 87 (1) (2007) 99–163.

[44] X. Dong, J. Fu, X.B. Yin, C.H. Qu, C.J. Yang, H. He, J. Ni, Induction of apoptosis in HepaRG cell line by aloe-emodin through generation of reactive oxygen species and the mitochondrial pathway, Cell. Physiol. Biochem. 42 (2) (2017) 685–696.

[45] N. Qin, S.Y. Lu, N. Chen, C.X. Chen, Q.Q. Xie, X.J. Wei, F.X. Ye, J.H. He, Y.C. Li, L.X. Chen, L.H. Jiang, X.Q. Lu, Y.C. Yuan, J. Li, Y. Jiao, R.B. Huang, Yulangsan polysaccharide inhibits 4T1 breast cancer cell proliferation and induces apoptosis *in vitro* and *in vivo*, Int. J. Biol. Macromol. 121 (2019) 971–980.

[46] D.T. Yin, M.Y. Lei, J.H. Xu, H.Q. Li, Y.F. Wang, Z. Liu, R.S. Ma, K. Yu, X.H. Li, The Chinese herb *Prunella vulgaris* promotes apoptosis in human well-differentiated thyroid carcinoma cells via the B-cell lymphoma-2/Bcl-2-associated X protein/caspase-3 signaling pathway, Oncol. Lett. 14 (2) (2017) 1309–1314.

[47] M. Huang, Y. Wang, L. Xu, M. You, Anti-tumor properties of *Prunella vulgaris*, Curr. Pharmacol. Rep. 1 (6) (2015) 401–419.

[48] Y.G. Song, L. Kang, S. Tian, L.L. Cui, Y. Li, M. Bai, X.Y. Fang, L.H. Cao, K. Coleman, M.S. Miao, Study on the anti-hepatocarcinoma effect and molecular mechanism of *Prunella vulgaris* total flavonoids, J. Ethnopharmacol. 273 (2021), 113891.

[49] J. Zhang, Y. Wang, H.D. Zhao, J. Zhang, X.C. Dong, C. Wang, J. Gao, H.Z. Zhang, Effects of traditional Chinese medicine *Prunella vulgaris* on proliferation cycle and apoptosis of human thyroid cancer cell Line SW579, Prog. Mod. Biomed. 11 (23) (2011) 4434–4436 (现代生物医学进展).

[50] D. Es-saady, A. Simon, M. Ollier, J.C. Maurizis, A.J. Chulia, C. Delage, Inhibitory effect of ursolic acid on B16 proliferation through cell cycle arrest, Cancer Lett. 106 (2) (1996) 193–197.

[51] T. Zhang, J.J. Li, Y.M. Dong, D. Zhai, L. Lai, F.J. Dai, H.Y. Deng, Y.H. Chen, M.Y. Liu, Z.F. Yi, Cucurbitacin E inhibits breast tumor metastasis by suppressing cell migration and invasion, Breast Cancer Res. Treat. 135 (2) (2012) 445–458.

[52] S.H. Kim, C.Y. Huang, C.Y. Tsai, S.Y. Lu, C.C. Chiu, K. Fang, The aqueous extract of *Prunella vulgaris* suppresses cell invasion and migration in human liver cancer cells by attenuating matrix metalloproteinases, Am. J. Chin. Med. 40 (3) (2012) 643–656.

[53] Y. Han, L. Ma, L. Zhao, W. Feng, X. Zheng, Rosmarinic inhibits cell proliferation, invasion and migration via up-regulating miR-506 and suppressing MMP2/16 expression in pancreatic cancer, Biomed. Pharmacother. 115 (2019), 108878.

[54] M. Woo, R. Hakem, C. Furlonger, A. Hakem, G. S Duncan, T. Sasaki, D. Bouchard, L.W. Lu, G. E Wu, C. J Paige, T. W Mak, Caspase-3 regulates cell cycle in B cells: a consequence of substrate specificity, Nat. Immunol. 4 (10) (2003) 1016–1022.

[55] C.M.S. Garcia, M.R. de Araújo, M.T.P. Lopes, M.A.N.D. Ferreira, G.D. Cassali, Morphological and immunophenotipical characterization of murine mammary carcinoma 4t1, Braz. J. Vet. Parasitol. 7 (3) (2014) 158–165.
[56] Q. Xie, Y. Liu, X. Li, The interaction mechanism between autophagy and apoptosis in colon cancer, Transl. Oncol. 13 (12) (2020), 100871.
[57] L. Feng, W. Au-Yeung, Y.H. Xu, S.S. Wang, Q. Zhu, P. Xiang, Oleanolic acid from *Prunella Vulgaris* L. induces SPC-A-1 cell line apoptosis via regulation of Bax, Bad and Bcl-2 expression, Asian Pac. J. Cancer Prev. APJCP 12 (2) (2011) 403–408.
[58] F. Lauthier, L. Taillet, P. Trouillas, C. Delage, A. Simon, Ursolic acid triggers calcium-dependent apoptosis in human Daudi cells, Anti Cancer Drugs 11 (9) (2000) 737–745.